Faraday Discussions

Accepted Manuscript

This manuscript will be presented and discussed at a forthcoming Faraday Discussion meeting. All delegates can contribute to the discussion which will be included in the final volume.

Register now to attend! Full details of all upcoming meetings: http://rsc.li/fd-upcoming-meetings

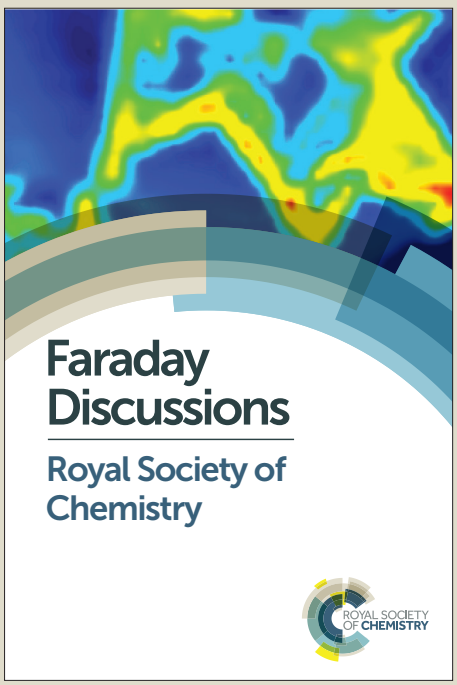

This is an *Accepted Manuscript*, which has been through the Royal Society of Chemistry peer review process and has been accepted for publication.

Accepted Manuscripts are published online shortly after acceptance, before technical editing, formatting and proof reading. Using this free service, authors can make their results available to the community, in citable form, before we publish the edited article. We will replace this *Accepted Manuscript* with the edited and formatted *Advance Article* as soon as it is available.

You can find more information about *Accepted Manuscripts* in the Information for Authors.

ROYAL SOCIETY OF CHEMISTRY

www.rsc.org/faraday_d

Proton uptake in the H^+-SOFC cathode material $Ba_{0.5}Sr_{0.5}Fe_{0.8}Zn_{0.2}O_{3-\delta}$: Transition from hydration to hydrogenation with increasing oxygen partial pressure

Daniel Poetzsch, Rotraut Merkle*, Joachim Maier
Max Planck Institute for Solid State Research, Stuttgart, Germany

Abstract

Thermogravimetric investigations on the perovskite $Ba_{0.5}Sr_{0.5}Fe_{0.8}Zn_{0.2}O_{3-\delta}$ (BSFZ, with mixed hole, oxygen vacancy and proton conductivity) from water vapor can occur by hydration (acid-base reaction) or hydrogenation (redox reaction), depending on the oxygen partial pressure, i.e. on the material's defect concentrations. In parallel, also the effective diffusion coefficient of the stoichiometry relaxation kinetics changes. These striking observations can be rationalized in terms of a defect chemical model and transport equations for materials with three mobile carriers. Implications for the search of cathode materials with mixed electronic and protonic conductivity for application on proton conducting oxide electrolytes are discussed.

1 Introduction

Amongst oxide-based fuel cells, cells based on proton-conducting electrolytes (abbreviated H^+-SOFC or PCFC) have a great potential as to reduce the operating temperature below 700 °C. This is essentially due to a higher ionic conductivity of the electrolyte compared to oxide ion conductors at given temperature,[1,2] and offers advantages such as faster startup, less degradation, and last but not least reduced cost (less expensive materials, e.g. less effort for sealing, bipolar plates). Furthermore, formation of water occurs at the cathode without diluting the fuel. However, reduced temperatures increase the overpotentials, in particular of the cathode process which typically shows the highest activation energy. For a high cathode performance it is feasible to use materials with mixed ionic and electronic conductivity because this increases the catalytically active zone beyond the triple-phase-boundary (TPB, where electrode, electrolyte and gas phase are in contact).[3] For the cathodes of H^+-SOFCs, materials with sufficiently high hole (p-type conducting in oxidizing atmosphere) and proton conductivity are desired. In the literature, as a first attempt perovskites which show mixed oxygen vacancy and hole conductivity (employed already as cathodes on YSZ) are used in the form of porous cathodes or porous composites mixed with the proton-conducting electrolyte,[4,5,6,7,8,9,10] and show good performances (the maximum power reported so far exceeds 2 W/cm^2 at 700°C[11]). However, these investigations do not provide direct evidence

for proton conductivity in the cathode materials (while the bulk proton conductivity of typical acceptor-doped $Ba(Zr,Ce)O_3$ electrolyte materials is in the range of 10^{-3} to $2\cdot10^{-2}$ S/cm at 300-600°C and 30 mbar H_2O[12]). Already the determination of the proton concentration in such materials is difficult, because - in contrast to the proton conducting electrolyte - more than one reaction may contribute to proton uptake as discussed in detail in section 2 and 3. Proton contents extracted from thermogravimetric measurements without considering these complications, e.g. in refs.[4,5], have to be considered with great care. A chemical method of determining proton concentrations such as Karl-Fischer titration is much more reliable, but limited to measuring quenched samples under ex-situ conditions.[13,14] In a recent publication we extracted proton concentrations in $Ba_{0.5}Sr_{0.5}Fe_{0.8}Zn_{0.2}O_{3-\delta}$ (BSFZ) from in-situ thermogravimetric measurements and full defect chemical modeling under low p_{O_2},[15] and could also determine a lower bound for the proton mobility. In the present article, we extend this thermogravimetric investigation to conditions of lower and higher p_{O_2} and rationalize the observed changes in the defect chemical behavior. A detailed discussion if the corresponding proton conductivity is expected to suffice for the "bulk path", as well as experimental results on dense BSFZ microelectrodes will be given elsewhere.[16]

2 Theory

In this section the defect chemistry of a material with three mobile carriers such as oxygen vacancies $V_O^{\bullet\bullet}$, protonic defects $OH_O^{\bullet}$ and electron holes $h^{\bullet}$ is briefly laid out. A more quantitative analysis together with numerical simulations of scenarios covering various types of materials can be found in ref.[17].

Thermodynamics – The equilibration of the perovskite with the gas phase is described by two reactions: Eq. (1) is the oxidation reaction where oxygen vacancies are filled by oxygen from the gas phase forming holes.

$$\tfrac{1}{2}\,O_2 + V_O^{\bullet\bullet} \rightleftharpoons O_O^{x} + 2\,h^{\bullet} \qquad K_O = \frac{[O_O^{x}][h^{\bullet}]^2}{p_{O_2}^{1/2}[V_O^{\bullet\bullet}]} \qquad (1)$$

Instead of activities, concentrations denoted by brackets are used, assuming ideally dilute defects as a first approximation for this general defect model. In a material without perceptible proton concentration this reaction (together with the electroneutrality condition) suffices to describe the defect chemistry. But for a material with the ability for proton incorporation in humid atmosphere a second reaction such as the hydration reaction (2) is required.

$$H_2O + V_O^{\bullet\bullet} + O_O^x \rightleftharpoons 2\ OH_O^{\bullet} \qquad K_W = \frac{[OH_O^{\bullet}]^2}{p_{H_2O}[O_O^x][V_O^{\bullet\bullet}]} \qquad (2)$$

Here, the oxygen vacancies are filled by dissociative absorption of water in the gas phase, and the transfer of the second proton to a regular lattice oxygen creates a second protonic defect. This reaction is a pure acid-base reaction not involving electronic defects. In proton conducting electrolytes with low redox activity (large bandgap, low electronic defect concentration) this is the only way of proton incorporation. But in redox-active cathode materials the combination of reactions (1) and (2) corresponds to

$$H_2O + 2\ O_O^x + 2\ h^{\bullet} \rightleftharpoons 2\ OH_O^{\bullet} + ½\ O_2 \qquad K_{W/O} = \frac{p_{O_2}^{1/2}[OH_O^{\bullet}]^2}{p_{H_2O}[O_O^x]^2[h^{\bullet}]^2} = \frac{K_W}{K_O} \qquad (3)$$

This reaction describes proton uptake by a redox reaction at the expense of holes and can thus be named "hydrogenation" (uptake of hydrogen, in contrast to water uptake by reaction (2) = hydration). By this reaction a hole-conducting cathode material could incorporate protons even if it had no oxygen vacancies. However, one of equilibria (1)-(3) is mathematically redundant for the description of the defects chemistry. For the defect-chemical calculations (neglecting defect interactions such as trapping) furthermore the electroneutrality condition is required ($[Acc'] =$ concentration of acceptor dopants):

$$[Acc'] = 2[V_O^{\bullet\bullet}] + [OH_O^{\bullet}] + [h^{\bullet}] \qquad (4)$$

Using eqs. (1),(2),(4) the concentrations of oxygen vacancies, protons and holes are calculated numerically as a function of $K_O p_{O_2}^{1/2}$ ("redox activity", i.e. potential to change the valence of the A or B cation) and $K_W p_{H_2O}$ (potential to take up protons) assuming an acceptor dopant concentration of unity and shown in a triple-logarithmic plot in Fig. 1(a). This plot represents a "materials map": depending on $K_O p_{O_2}^{1/2}$ and $K_W p_{H_2O}$ values and the resulting major defect (and corresponding conductivity), one can recognize different materials classes: (1) Oxide ion conducting electrolytes such as $(La,Sr)(Ga,Mg)O_{3-x}$, (2) proton conducting electrolytes such as $(Ba,Sr)(Zr,Ce,Y)O_{3-x}$, (3) mixed oxide ion/hole conducting electrodes such as $(La,Sr)(Co,Fe)O_{3-\delta}$, and finally (4) mixed proton/hole conducting electrodes such as BSFZ, the desired case for cathodes on proton conducting electrolytes.

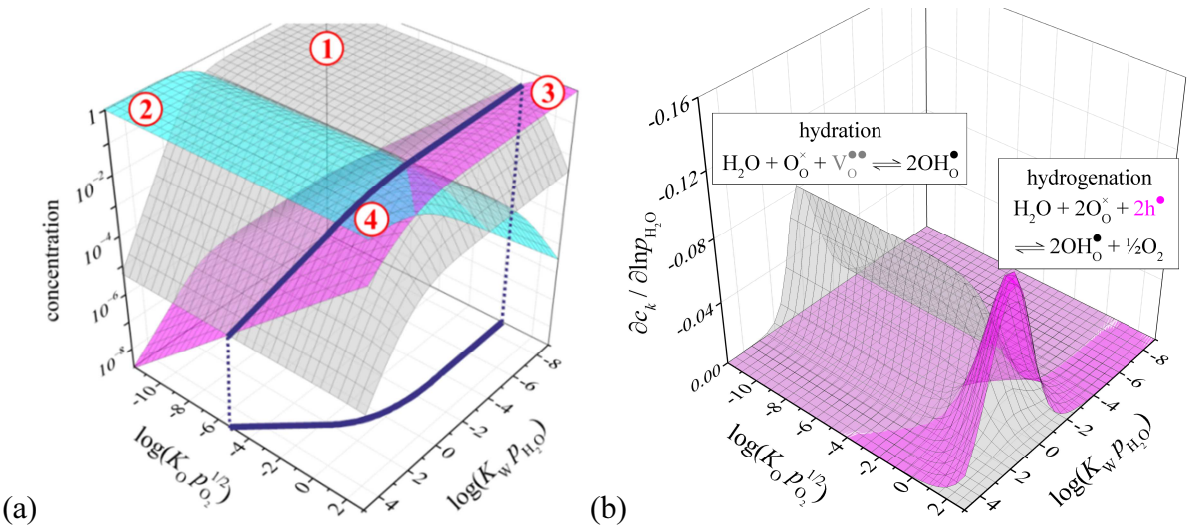

Figure 1: (a) Defect concentrations calculated from eq. (1), (2) and electroneutrality condition (4) with an acceptor concentration of 1 (grey surface = $[V_O^{\bullet\bullet}]$, blue surface = $[OH_O^\bullet]$, pink surface = $[h^\bullet]$). Different materials classes (1) = oxide electrolytes, (2) = proton electrolytes, (3) = mixed $V_O^{\bullet\bullet}/h^\bullet$ conductors and (4) = mixed $OH_O^\bullet/V_O^{\bullet\bullet}/h^\bullet$ conductors can be recognized in this "materials map". The blue line indicates the intersection of the grey and pink surface, i.e. the condition $[V_O^{\bullet\bullet}] = [h^\bullet]$. (b) Changes of $V_O^{\bullet\bullet}$ (grey surface) and $h^\bullet$ concentrations (pink surface) upon p_{H_2O} increase as calculated from the general defect model. Reproduced with permission from ref.[17], copyright Wiley-VCH (2015).

As discussed above, in $OH_O^\bullet/V_O^{\bullet\bullet}/h^\bullet$ mixed conductors, protons can be incorporated by hydration (eq. (2), proton uptake compensated by annihilation of $V_O^{\bullet\bullet}$) and/or hydrogenation (eq. (3), proton uptake compensated by annihilation of $h^\bullet$). From the general defect chemical model the concentration changes of $V_O^{\bullet\bullet}$ and $h^\bullet$ upon increasing pH_2O can be calculated. In Fig. 1(b) one can recognize that in the region of the electrolyte materials proton uptake is mainly compensated by $V_O^{\bullet\bullet}$ annihilation (grey surface corresponding to $\partial \ln[V_O^{\bullet\bullet}]/\partial \ln p_{H_2O}$ is higher than pink surface $\partial \ln[h^\bullet]/\partial \ln p_{H_2O}$), i.e. proton uptake occurs by the hydration reaction (2). For materials with high redox-activity located close to the right front edge of the materials map, proton uptake is mainly compensated by hole consumption, i.e. according to reaction (3). The border between both regimes approximately follows the line where the hole equals the oxygen vacancy concentration marked as bold blue line in Fig. 1(a) (strictly speaking the condition is $2[V_O^{\bullet\bullet}] = [h^\bullet]$;[18] additional deviations are to be expected when activities differ from concentrations).

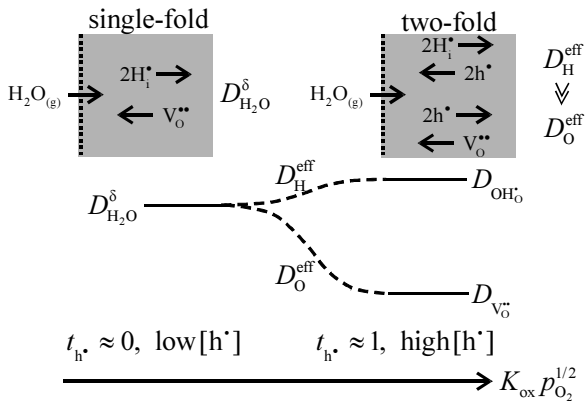

Figure 2: Change of stoichiometry relaxation process after increase of p_{H_2O} at constant p_{O_2}. Left: The situation with only two carriers (low hole concentration) can be described by a single chemical diffusion coefficient of water. Right: Materials with perceptible concentration of mobile holes show two-fold relaxation of fast hydrogen uptake followed by slower re-oxidation. Reproduced with permission from ref.[17], copyright Wiley-VCH (2015).

The presence of a third mobile carrier does not only lead to a more complex equilibrium defect chemistry, but even more to complications in stoichiometry relaxation kinetics (assumed here to be diffusion controlled, i.e. fast surface reaction). In the case of two carriers, local electroneutrality directly couples their fluxes, leading to a chemical diffusion coefficient of the neutral component which takes a value in-between the two respective defect diffusivities (in absence of trapping effects[19]). In the presence of an additional mobile carrier, only all three defects together have to fulfill electroneutrality, with the consequence that the defect fluxes are not directly coupled by simple prefactors any more, and quite complex diffusion kinetics may occur. For example, in the case of water incorporation the flux of highly mobile protons can transiently be charge compensated by electronic carriers such as holes, instead of "waiting" for the less mobile $V_O^{\bullet\bullet}$. Experimentally, a two-fold relaxation after a p_{H_2O} increase was observed in Fe-doped $SrTiO_3$ single crystals (showing up as peculiar non-monotonic changes in electrical conductivity and space-resolved optical absorption[20]) and alkali earth cerates and zirconates under certain conditions.[21,22] In a first approximation, water uptake becomes decoupled into a fast hydrogenation (uptake of protons and electrons, or annihilation of holes) followed by a slower oxidation process which brings the sample from an over-reduced intermediate state to its final equilibrium stoichiometry, cf. Fig. 2. First attempts of quantification were able to reproduce some of the characteristics,[21,23,24,25] however still exhibited shortcomings. Exact transport equations for this three carrier situation were derived in ref.[17] and complemented by numerical simulation examples. The carrier fluxes J_i are proportional to the respective gradients in electrochemical potential[26]

$$\begin{pmatrix} J_{V_O^{\bullet\bullet}} \\ J_{OH_O^{\bullet}} \\ J_{h^{\bullet}} \end{pmatrix} = -\frac{1}{F^2}\begin{pmatrix} \sigma_{V_O^{\bullet\bullet}}/4 & 0 & 0 \\ 0 & \sigma_{OH_O^{\bullet}} & 0 \\ 0 & 0 & \sigma_{h^{\bullet}} \end{pmatrix}\begin{pmatrix} \nabla\tilde{\mu}_{V_O^{\bullet\bullet}} \\ \nabla\tilde{\mu}_{OH_O^{\bullet}} \\ \nabla\tilde{\mu}_{h^{\bullet}} \end{pmatrix}. \quad (5)$$

Using the electroneutrality condition for three carriers $J_{V_O^{\bullet\bullet}} + J_{OH_O^{\bullet}} + J_{h^{\bullet}} = 0$ and expressing the chemical potentials by concentrations via $\mu_k = \mu_k^0 + RT\ln c_k$ (in the ideally dilute limit) finally yields expressions in which the defect fluxes are unambiguously related to the concentration gradients ($D_{V_O^{\bullet\bullet}}$, $D_{OH_O^{\bullet}}$, $D_{h^{\bullet}}$ denote the defect diffusivities, $t_{V_O^{\bullet\bullet}}$, $t_{OH_O^{\bullet}}$, $t_{h^{\bullet}}$ are the respective transference numbers):

$$J_{V_O^{\bullet\bullet}} = -\left[(1-t_{V_O^{\bullet\bullet}})D_{V_O^{\bullet\bullet}} + t_{V_O^{\bullet\bullet}}D_{h^{\bullet}}\right]\nabla c_{V_O^{\bullet\bullet}} - ½\left[t_{V_O^{\bullet\bullet}}(D_{h^{\bullet}} - D_{OH_O^{\bullet}})\right]\nabla c_{OH_O^{\bullet}} \quad (6)$$

$$J_{OH_O^{\bullet}} = -2\left[t_{OH_O^{\bullet}}(D_{h^{\bullet}} - D_{V_O^{\bullet\bullet}})\right]\nabla c_{V_O^{\bullet\bullet}} - \left[(1-t_{OH_O^{\bullet}})D_{OH_O^{\bullet}} + t_{OH_O^{\bullet}}D_{h^{\bullet}}\right]\nabla c_{OH_O^{\bullet}} \quad (7)$$

$$J_{h^{\bullet}} = -(-2)\left[t_{h^{\bullet}}D_{V_O^{\bullet\bullet}} + (1-t_{h^{\bullet}})D_{h^{\bullet}}\right]\nabla c_{V_O^{\bullet\bullet}} - (-1)\left[t_{h^{\bullet}}D_{OH_O^{\bullet}} + (1-t_{h^{\bullet}})D_{h^{\bullet}})\right]\nabla c_{OH_O^{\bullet}} \quad (8)$$

The third equation is redundant and given for completeness only. These expressions show that the flux of one carrier (e.g. $V_O^{\bullet\bullet}$ given by (6)) depends on its "own" concentration gradient as well as on a second gradient ($\nabla c_{OH_O^{\bullet}}$ in (6)) which is not coupled to the "own" gradient by a simple prefactor ($\nabla c_{V_O^{\bullet\bullet}} = -½\nabla c_{OH_O^{\bullet}}$ as for a system containing only $V_O^{\bullet\bullet}$ and $OH_O^{\bullet}$ is not valid here any more, instead only $2\nabla c_{V_O^{\bullet\bullet}} + \nabla c_{OH_O^{\bullet}} + \nabla c_{h^{\bullet}} = 0$ holds). It is important to note that the peculiar kinetic behaviors possible in such three carrier systems (two-fold non-monotonic relaxation) occur already at small driving forces. They arise from the additional degree of freedom given by the fact that only all three carriers together have to fulfill electroneutrality, not from concentration-dependent diffusivities under high driving forces.

3 Experimental

To avoid complications from water surface adsorption, and to be able to extract diffusion coefficients after partial pressure changes, BFSZ was used in the form of dense pellets for thermogravimetry. BSFZ powder prepared by a modified Pechini method was compacted using spark plasma sintering in graphite dies under Ar atmosphere (FCT Systeme, Germany, 1050 °C with 300 K/min, 50 MPa pressure, holding 2 min). The pellets were ground from both sides to slices of 1.5 mm thickness, 5-10 mm lateral dimension . Densities of about 97% were obtained, sufficient to ensure that the diffusion length equals the sample thickness.[27] For

the oxygen exchange reaction (1) this thickness ensures that stoichiometry relaxation is in the diffusion controlled (critical thickness of related perovskites is much lower than 1 mm [28]); for reactions (2) and (3) which may proceed by a different reaction mechanism such a value is not available, but one can reasonably assume there reactions to proceed at comparable or higher rate (e.g. (2) does not require dissociation of the O=O bond in O_2).

Oxygen deficiency (and thus $[V_O^{\bullet\bullet}]$ and $[h^{\bullet}]$) under dry conditions were extracted from thermogravimetry (STA449C Jupiter TG, Netzsch, Germany) by stepwise changes of temperature and p_{O_2}. The absolute O stoichiometry of a quenched sample was determined using iodometric titration.[27] The proton concentration and the relaxation behavior were analyzed after stepwise changes in p_{H_2O} from 5.7 to 9.8 and 14.5 mbar (by changing the temperature of the humidifier, monitored by a HygroClip sensor (Rotronic, Germany)) under different oxygen partial pressures. Since the relative weight changes of the p_{H_2O} steps are very small, ≈ 4 g of BSFZ pellets were used in these measurements to obtain sufficient precision. For p_{H_2O} changes buoyancy effects were found to be negligible, for T and p_{O_2} changes they were corrected based on a measurement with an empty crucible (even there the corrections are small compared to sample weight changes).

For an independent determination of the proton content, BSFZ pellets which had already numerous cracks (and thus equilibrated much faster that the samples used for stoichiometry relaxation in thermogravimetry) were equilibrated at given T, p_{O_2} and p_{H_2O} and rapidly quenched. The water content was measured by rapidly heating the sample to 600 °C in a gas stream of dry argon and analyzing the output gas by Karl-Fischer titration.[27] Total conductivity (≈ hole conductivity) was measured by 4-point-DC (2400 Digital Sourcemeter, Keithley, USA) on a bar-shaped SPS sintered sample in dry, oxidizing atmosphere.

Details of the finite difference numerical simulations of the stoichiometry relaxation kinetics based on eqs. (6-8) can be found in ref.[17]. The input parameters are the defect diffusivities and the initial and final defect concentrations.

4 Results and Discussion

4.1 Dry conditions

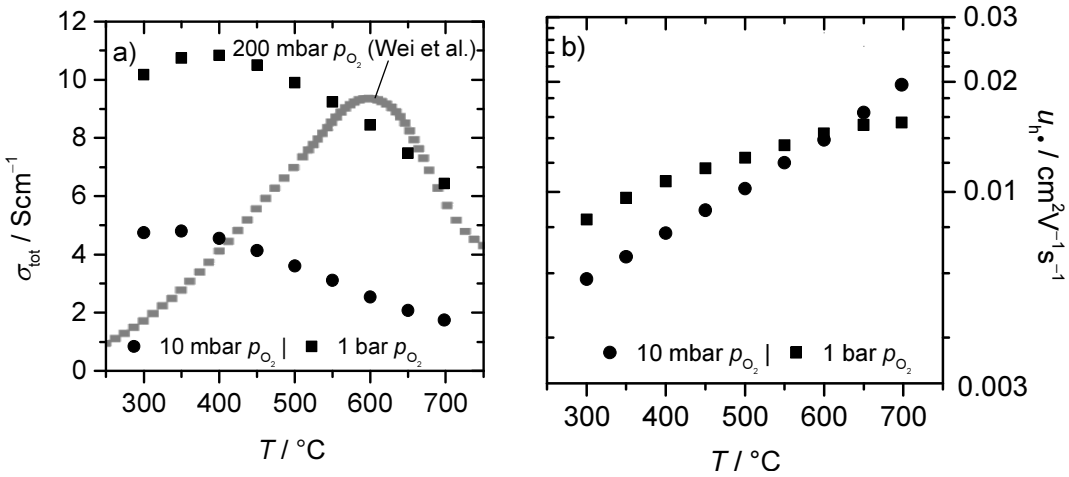

Figure 3: (a) Total conductivity ≈ hole conductivity of BSFZ in dry atmosphere. The black symbols are measured under conditions equilibrated with p_{O_2} = 0.01 or 1 bar, while the grey squares taken from ref. [29] were apparently obtained without equilibration of the sample. (b) Hole mobility calculated from σ_{tot} and $[h^\bullet]$ in Fig. 4(a).

BSFZ is a perovskite with predominant p-type electronic conduction as illustrated in fig. 3(a). In such a perovskite with a high concentration of redox-active transition metals, the holes can be identified with Fe^{4+} on Fe^{3+} sites ($Fe^{\bullet}_{Fe}$). Typically, Fe-based perovskites exhibit polaron hopping.[30] In agreement with this expectation, the hole mobility (calculated from σ_{tot} and the hole concentration in fig. 4a) is found to be thermally activated. Thus the decrease of σ_{tot} with increasing temperature is caused by the decrease of the hole concentration with increasing *T*.

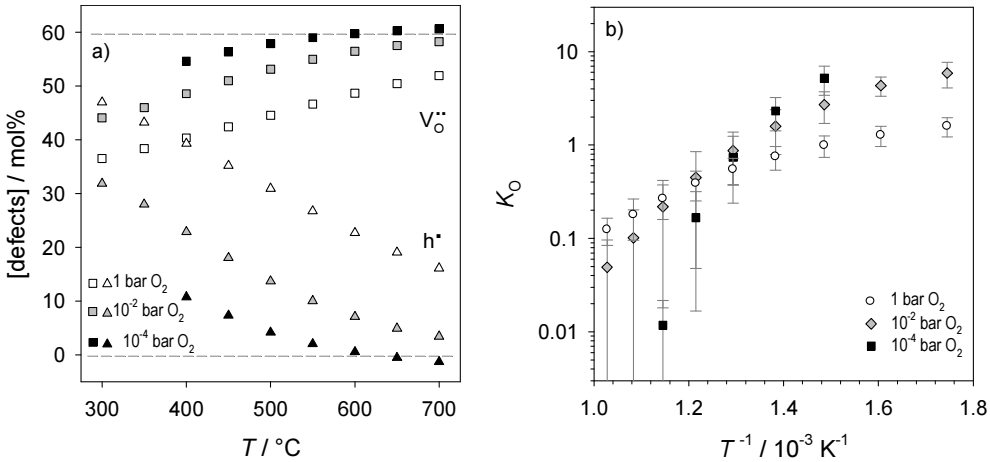

Figure 4: (a) $V_O^{\bullet\bullet}$ (squares) and $h^\bullet$ concentrations (triangles) in BSFZ in dry p_{O_2} = 10^{-4}, 10^{-2} or 1 bar as determined from thermogravimetry (error bar ≈ symbol size). Data for p_{O_2} = 10^{-2} bar previously published in [15]. (b) Mass action constant K_O of oxygen exchange reaction (1) calculated from $[V_O^{\bullet\bullet}]$ and $[h^\bullet]$ under dry conditions.

The $V_O^{\bullet\bullet}$ and $h^{\bullet}$ concentrations determined from thermogravimetry in dry 10^{-4}, 10^{-2} and 1 bar O_2 are shown in Fig. 4(a). Under dry conditions the hole concentration is obtained from the measured $[V_O^{\bullet\bullet}]$ and the electroneutrality condition $[Acc']=2[V_O^{\bullet\bullet}]+[h^{\bullet}]$ with $[Acc']=1.2$ (the perovskite's A-site is fully acceptor doped by Ba and Sr, and additionally 20% Zn^{2+} on replacing Fe^{3+} on the B site further increases the acceptor concentration). These oxygen nonstoichiometry values are in good agreement with measurements in 0.2 bar O_2.[29] The dashed lines in Fig. 4(a) indicate the $V_O^{\bullet\bullet}$ and $h^{\bullet}$ concentrations for BSFZ when all iron is in +3 oxidation state. Obviously, this plateau is reached in 10^{-4} bar O_2 at temperatures ≥ 600 °C (cf. the plateaus in $V_O^{\bullet\bullet}$ concentration observed for $La_{1-x}Sr_xO_{3-\delta}$ perovskites, indicating that a reduction to Fe^{2+} is not favorable[31]). The mass action constants K_O for the oxygen exchange reaction (1) calculated from $[V_O^{\bullet\bullet}]$ and $[h^{\bullet}]$ are shown in Fig. 4(b). It is obvious that the data points do not follow a straight line as expected under the assumption that the standard reaction enthalpy and entropy ΔH_O^0 and ΔS_O^0 are T-independent in the covered temperature range. Also, even if a straight line was fitted to the data, the slopes would obviously increase with decreasing p_{O_2} (i.e. the corresponding apparent ΔH_O^0 becomes more negative). This indicates that $V_O^{\bullet\bullet}$ and $h^{\bullet}$ in BSFZ do not behave as ideally dilute defects (which is not surprising given that one of these defect concentrations is always high, and the temperatures are comparably low). Tentatively fitting a straight line to K_O vs T^{-1} at an intermediate p_{O_2} = 10^{-2} bar yields $\Delta H_O^0 = -0.6\,\text{eV}$, which is in the same range as ΔH_O^0= -(0.6-0.7 eV) for $Ba_{0.5}Sr_{0.5}FeO_{3-\delta}$.[32]

4.2 Humid conditions

Proton uptake of BSFZ was investigated thermogravimetrically by stepwise changes of p_{H_2O} while temperature and p_{O_2} were kept constant. Under all investigated p_{O_2} a p_{H_2O} increase leads to a weight increase of the sample. However, there are two striking differences as depicted in Fig. 5(a) and (b): (i) the weight changes Δm under low p_{O_2} (10^{-2} and 10^{-4} bar) are much larger than in pure O_2, (ii) the relaxation process is much slower in low p_{O_2} compared to pure O_2. This difference can be related to the different possibilities of proton uptake for redox-active materials as outlined in Section 2, i.e. a change from hydration (reaction (2)) with subsequent chemical diffusion of water into the sample under low p_{O_2} conditions, to

predominant proton uptake by hydrogenation (reaction (3)) with corresponding chemical diffusion of hydrogen which is expected to be faster than water diffusion.

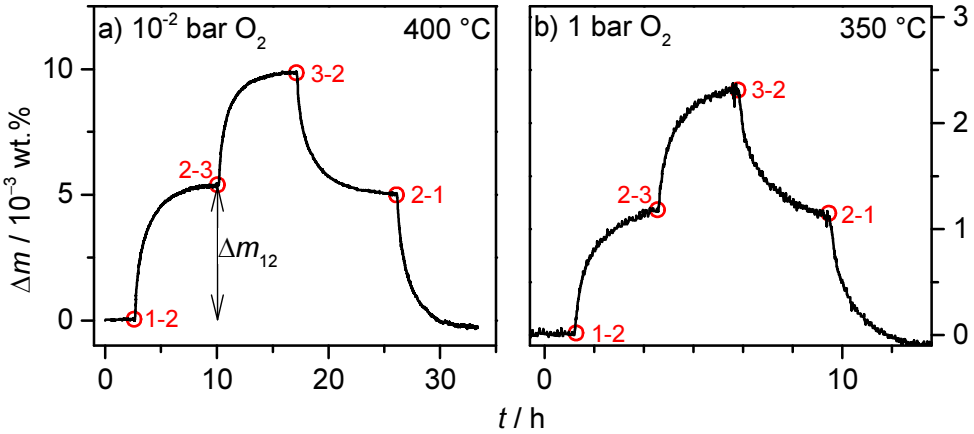

Figure 5: Weight relaxation of 1.5 mm thick BSFZ pellets after p_{H_2O} steps from 5.7 to 9.8 and 14.5 mbar. The red circles indicate the time of switching between the different p_{H_2O}. (a) in p_{O_2} = 10^{-2} bar at 400 °C (data taken from ref.[15]). (b) in p_{O_2} = 1 bar at 350 °C. Please note the smaller range on the x and y-axis; the smaller Δm reflects also in the noise becoming more visible.

Let us analyze this transition in detail, first regarding the equilibrium defect concentrations. As discussed in the previous publication,[15] fitting the weight changes in p_{O_2} = 10^{-2} bar by the full defect chemical model (comprising acid-base and redox reactions) results in proton uptake mainly occurring by the hydration reaction (2), i.e. the proton uptake is mainly compensated by $V_O^{\bullet\bullet}$ annihilation. The resulting proton concentrations are shown in Fig. 6(a). Since in p_{O_2} = 10^{-4} bar $[V_O^{\bullet\bullet}]$ further increases compared to 10^{-2} bar while $[h^{\bullet}]$ decreases (Fig. 4(a)), the general defect chemical considerations shown in Fig. 1(b) indicate a negligible contribution from the hydrogenation reaction (3). Thus these weight changes were directly fitted with the hydration reaction (2) only. The black symbols in Fig. 6(a) show that this very low p_{O_2} leads to moderately increased proton concentrations compared to p_{O_2} = 10^{-2} bar.

In pure oxygen, the situation differs strongly. The general defect model (Fig. 1) predicts that with increasing p_{O_2} at some point the proton uptake will change from predominant hydration (2) to hydrogenation reaction (3), and the drastic decrease of Δm in combination with shorter relaxation times indicates this change of proton uptake reaction occurred between 10^{-2} bar and 1 bar O_2. Furthermore, if the sample is exposed to D_2O instead of H_2O, the weight changes between corresponding p_{D_2O} are significantly larger (typically by a factor of 1.5-1.8) than for the respective p_{H_2O} changes. This comes close to the factor of two expected in case of pure hydrogenation (under the assumption of $[OH_O^{\bullet}]$=$[OD_O^{\bullet}]$), and is clearly different from

p_{D_2O} and p_{H_2O} changes in p_{O_2} = $10^{-2} \leq 10^{-2}$ bar where Δm_{D2O} exceeds Δm_{H2O} only slightly by a factor of 1.05 (which is essentially still within the error bar because of the very small weight changes in pure O_2; expected ratio for water uptake is 20/18=1.1). However, while this argument qualitatively supports predominant hydrogenation, it should not be attempted to quantitatively extract a ratio between hydration and hydrogenation reaction from Δm_{D2O} versus Δm_{H2O} (ΔH_W^0 and ΔS_W^0 could differ between H and D, leading to differences in equilibrium proton, deuterium concentrations even for identical partial pressures).

The proton concentrations in 1 bar O_2 were extracted from the TG results based on the hypothesis of exclusive hydrogenation by reaction (3). They are shown in Fig. 6(a) as open symbols, and are comparable to $[OH_O^\bullet]$ in p_{O_2} = 10^{-2} bar. This interpretation is also supported by the comparison of these in-situ measured $[OH_O^\bullet]$ with results from Karl-Fischer titration on samples quenched from equilibration with 20 mbar H_2O and 1 bar O_2 (red stars in Fig. 6(a)) which agree well with the TG data.

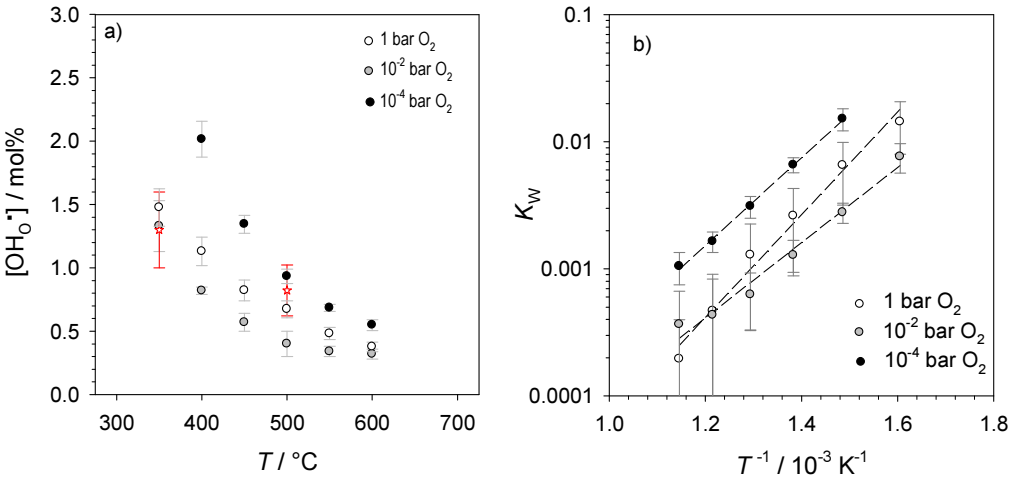

Figure 6: (a) Proton concentrations of BSFZ in p_{H_2O} = 20 mbar and different p_{O_2}, obtained from the analysis of p_{H_2O} changes in the thermogravimetry. The red stars are obtained from Karl-Fischer titration on samples quenched from p_{H_2O} = 20 mbar and p_{O_2} = 1 bar. Data for p_{O_2} = 10^{-2} taken from ref. [15]. (b) Hydration mass action constant K_W calculated from the defect concentrations in (a), plotted versus inverse temperature.

Unfortunately, application of the fitting routine with the defect model comprising the acid-base and redox reaction (as done for p_{O_2} = 10^{-2} bar, now using K_O determined from dry pure O_2) does not lead to a consistent result in 1 bar O_2 (it still yields largely proton uptake by hydration, which means that the proton concentrations would be lower by a factor of 9 - obviously contradicting the Karl-Fischer titration result). This can be traced back to the fact that - in lack of actual values - in the defect model the activities are replaced by

concentrations (the non-unity activity coefficients are implicitly absorbed into the mass action constants). However, as shown in Fig. 4(b), p_{O_2} -dependent nonidealities are important for $[V_O^{\bullet\bullet}]$ and/or $[h^\bullet]$, but they are not properly transferred from the measurement of K_O to the application in K_W because one cannot unambiguously quantify individual activity coefficients for $V_O^{\bullet\bullet}$ and $h^\bullet$. The activity of $h^\bullet$ appears to increase more strongly than their concentration when going from 10^{-2} to 1 bar O_2 (but the apparent K_O which reflects only the concentration change is lower in 1 bar O_2 compared to 10^{-2} bar) which leads to the change of the dominant proton uptake reaction. In view of these considerations, we note that the proton concentration determined in p_{O_2} = 10^{-2} bar might slightly be underestimated. But with a potential underestimation of $[OH_O^\bullet]$ we stay on the safe side in answering the question if the proton conductivity of BSFZ as cathode material suffices for oxygen reduction by the bulk path.

The values of the hydration mass action constant K_W calculated from the defect concentrations are plotted in Fig. 6(b) versus inverse temperature (even if proton uptake in pure O_2 actually proceeds by hydrogenation reaction (3), K_W values can still be calculated). In contrast to K_O in Fig. 4(b), for a given p_{O_2} the K_W values follow a straight line, i.e. the protons behave as dilute defects. The nonidealities of $V_O^{\bullet\bullet}$ and $h^\bullet$ can be absorbed in activity coefficients deviating from one, which depend on p_{O_2} but are, however, independent of p_{H_2O} (i.e. independent of the low $[OH_O^\bullet]$). The standard hydration enthalpy ΔH_W^0 extracted from the slopes amounts to -0.7±0.15 eV. Fig. 7 compares ΔH_W^0 and ΔS_W^0 values for BSFZ with data measured for barium zirconate and cerate electrolyte materials.[12] While ΔH_W^0 and ΔS_W^0 individually fall within the range of the electrolyte perovskites, the combination of ΔH_W^0 and ΔS_W^0 for BSFZ results in a less negative free enthalpy ΔG_W^0, corresponding to the lower proton content of BSFZ. Further investigations (experimental as well as ab initio calculations) are required to understand which materials parameters are decisive for the proton concentration in such mixed conducting perovskites (and responsible for the lower $[OH_O^\bullet]$ compared to the electrolytes). A decreased basicity of the oxygen related to a more covalent Fe-O bonding (compared to Zr-O and Ce-O in electrolytes) might be one reason. Nonetheless, as discussed in ref.[15] and experimentally demonstrated on dense BSFZ microelectrodes[16] the proton concentration in BSFZ gives rise to a proton conductivity which suffices for oxygen reduction by the "bulk path".

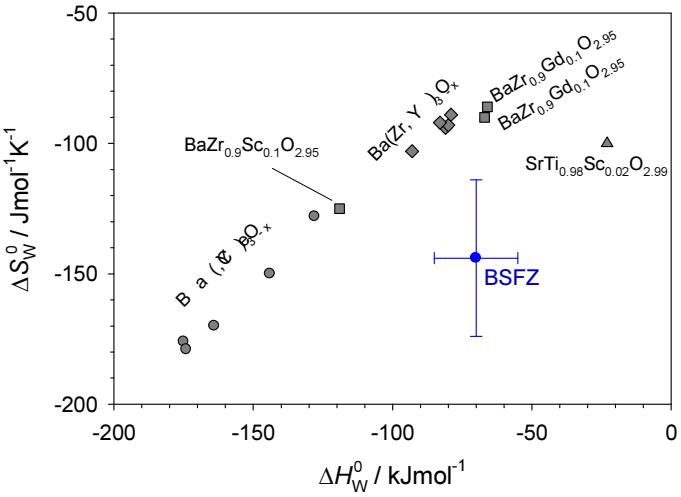

Figure 7: Standard enthalpies and entropies of the hydration reaction (2) for several barium zirconate and barium cerate electrolyte materials (data taken from ref.[12]; for materials families comprising different acceptor concentrations the oxygen deficiency amounts to [$V_O^{\bullet\bullet}$] = 0.5 [A']). The data obtained for BSFZ in the present study are overlaid in blue. So far BSFZ is the only cathode material for which ΔH_W^0 and ΔS_W^0 were determined.

4.3 Stoichiometry relaxation kinetics

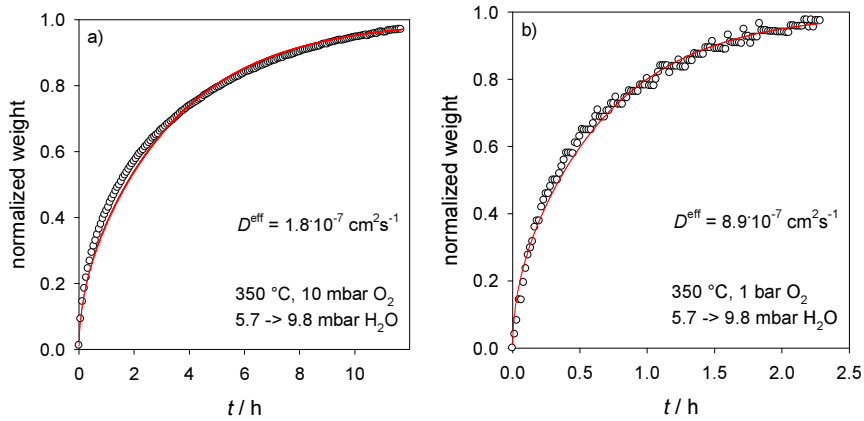

Figure 8: Relaxation of normalized weight of the 1.5 mm thick BSFZ pellets (symbols) after p_{H_2O} increase from 5.7 to 9.8 mbar at 350 °C. (a) in p_{O_2} = 10^{-2} bar, (b) in p_{O_2} = 1 bar. The solid lines represent the fit curve.

Let us now analyze the diffusion kinetics of stoichiometry relaxation in more detail. Fig. 8 shows exemplary fits of normalized weight changes after p_{H_2O} increase. These curves can reasonably well be fitted with a single, constant effective diffusion coefficient D_m^{eff}.[33] The resulting D_m^{eff} and overall weight changes Δm for a p_{H_2O} step are collected in Fig. 9, showing that D_m^{eff} as well as Δm strongly vary with p_{O_2}. As discussed in the previous section, the decrease of Δm at higher p_{O_2} can be traced back to the change from predominant hydration reaction to hydrogenation reaction with increasing hole activity. It is interesting to note that at high p_{O_2} the extracted diffusion coefficient is close to the proton diffusivity in

$Ba(Zr_{0.9}Y_{0.1})O_{2.95}$ (blue dashed line in fig. 9(a), E_a = 0.44 eV), while at low p_{O_2} it is in the range of $D_{V_O^{\bullet\bullet}}$ (grey dashed line, E_a = 0.62 eV). Overall, the diffusion kinetics is in line with the interpretation in terms of changes from hydrogenation to hydration, but the detailed analysis becomes somewhat more involved.

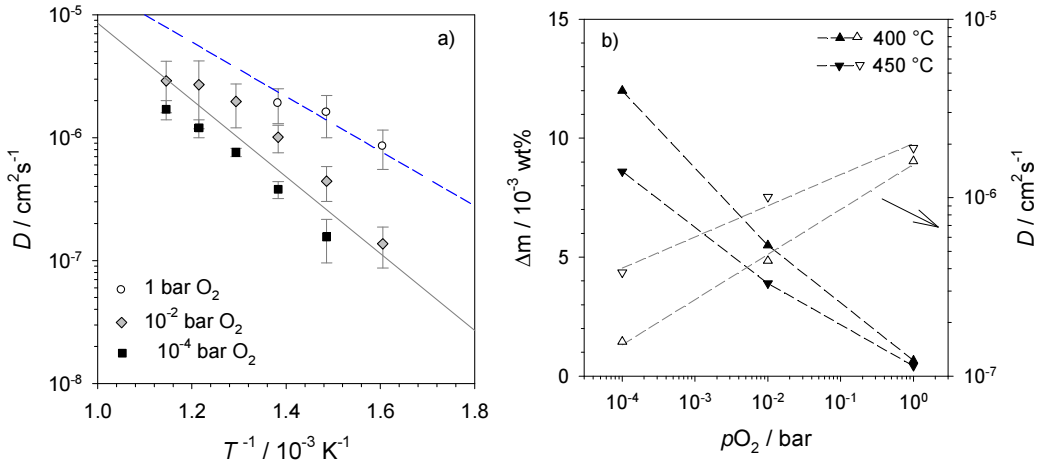

Figure 9: (a) Effective diffusion coefficients D_m^{eff} for p_{H_2O} changes as obtained from the single-parameter fit of thermogravimetric relaxation in different p_{O_2}. The dashed blue line indicates the bulk proton diffusivity of $Ba(Zr_{0.9}Y_{0.1})O_{2.95}$ taken from ref.[12], the solid grey line the $V_O^{\bullet\bullet}$ diffusivity calculated from O permeation measurements on BSFZ.[34]. (b) Weight changes Δm for p_{H_2O} increase from 5.7 to 9.8 mbar (solid symbols), and effective diffusivities D_m^{eff} (open symbols) plotted as function of p_{O_2} (lines are guide to the eye only).

The first point to be discussed is that based on the general considerations in section 2, one should expect to observe two relaxation processes with different time scale (at least under some p_{O_2} conditions). Mathematically, the relaxation curves could be fitted with a linear combination of two diffusion processes (D_O^{eff} and D_H^{eff}), but owing to the low weight contribution of proton concentration changes relative to O, the errors of the resulting D_H^{eff} are so large that these values are not meaningful in the present case. Only if the total weight increase is indeed dominated by H uptake at sufficiently high p_{O_2}, i.e. the p_{H_2O} increase mainly leads to chemical diffusion of hydrogen, a reliable D_H^{eff} value is obtained from fitting the relaxation curve with a single diffusivity. This behavior will now be illustrated by numerical simulations.

In ref.[17], the exact transport equations for the case of three mobile carriers were derived, and some numerical examples given. Here we use the same approach. However, we face two complications: (i) as discussed in section 4.2, with respect to the hole activity BSFZ does obviously not behave as an ideally dilute system. Thus, to cover the regimes of predominant

hydration as well as hydrogenation, we have to extend the range of $K_O p_{O_2}^{1/2}$ values beyond those covered experimentally (where the apparent K_O reflects the concentrations, not activities). (ii) Under conditions of low p_{O_2} the influence of holes on the diffusion processes becomes negligible and the relaxation becomes determined by the chemical diffusion coefficient of water $D^{\delta}_{H_2O}$. $D^{\delta}_{H_2O}$ is given by $D^{\delta}_{H_2O} = (1-t_{OH^{\bullet}_O})D_{OH^{\bullet}_O} + t_{OH^{\bullet}_O} D_{V^{\bullet\bullet}_O}$ with $t_{OH^{\bullet}_O}$ = proton transference number, i.e. for the low degree of hydration in BSFZ ($[OH^{\bullet}_O] < [V^{\bullet\bullet}_O]$, Fig. 6) one should expect that $D^{\delta}_{H_2O} \approx D_{OH^{\bullet}_O}$ (cf. ref. [35]). But Fig. 9(a) indicates that at low p_{O_2} the effective diffusivity rather approaches $D_{V^{\bullet\bullet}_O}$ than proton diffusivity - the material behaves as if it had a high degree of hydration (i.e. only a fraction of all lattice oxygens might be preferred sites for protonation. An increase of $[OH^{\bullet}_O]$ by a constant factor at all T would make ΔS^0_W less negative but leave ΔH^0_W unchanged). Thus, also the proton concentration and/or mobility seems affected by defect interactions.

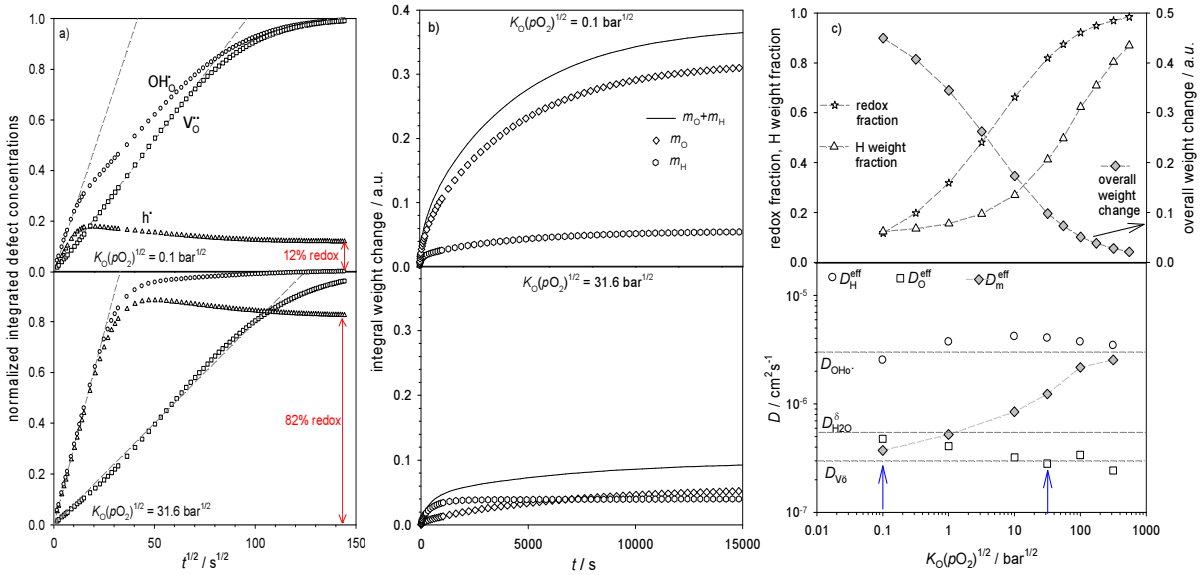

Figure 10: Results from numerical simulations of p_{H_2O} changes (10 to 20 mbar) at 450 °C for different $K_O p_{O_2}^{1/2}$ values calculated with $D_{V^{\bullet\bullet}_O}$ = 3·10^{-7} cm^{2}s^{-1}, $D_{OH^{\bullet}_O}$ = 3·10^{-6} cm^{2}s^{-1}, $D_{h^{\bullet}}$ = 5·10^{-4} cm^{2}s^{-1}. (a) Changes of normalized defect concentrations, the red arrows indicate the fraction of proton uptake which occurs by redox reaction (3). With the applied $t^{1/2}$ scale, for small times diffusion processes appear as a straight line. (b) Total weight increase (line) and individual O and H contributions (symbols) versus time. (c) Top: Fraction of proton uptake by redox reaction, overall weight change Δm and H contribution to Δm upon increased p_{H_2O}. Bottom: effective diffusivities D^{eff}_O, D^{eff}_H, D^{eff}_m extracted from the slopes of $[V^{\bullet\bullet}_O]$, $[OH^{\bullet}_O]$ and normalized weight versus $t^{1/2}$ (the blue arrows indicate the conditions of (a),(b)); the dashed lines give defect diffusivities $D_{V^{\bullet\bullet}_O}$, $D_{OH^{\bullet}_O}$ and the value the water chemical diffusion coefficient $D^{\delta}_{H_2O}$ would take in absence of holes.

Therefore, the input parameters for calculation of defect concentrations (ideally dilute model) have to be somewhat modified compared to the K_O and K_W values in Figs. 4, 6 (higher degree of hydration i.e. higher $K_W p_{H_2O}$ value, larger $K_O p_{O_2}^{1/2}$ range). The defect diffusivities correspond to values for BSFZ ($D_{V_O^{\bullet\bullet}}$, $D_{h^\bullet}$) and $Ba(Zr_{0.9}Y_{0.1})O_{2.95}$ ($D_{OH_O^\bullet}$) at 450 °C. Fig. 10(a) gives examples of the defect concentration changes after p_{H_2O} increase for conditions of low (top panel) and high (bottom panel) p_{O_2} , the corresponding weight changes are shown in Fig. 10(b). At low p_{O_2} , the p_{H_2O} increase mainly leads to proton uptake by the hydration reaction (the fraction of protons taken up by redox reaction (3) as indicated by the red arrow is small), and the proton and $V_O^{\bullet\bullet}$ concentrations have almost the same time behavior (the hole concentration is still too low for perceptible decoupling of H and O transport). The weight increase is dominated by the contribution from O, and the effective diffusion coefficient D_m^{eff} fitted from the normalized weight change (Fig. 10(b)) is close to $D_{H_2O}^{\delta}$ ($\approx D_{V_O^{\bullet\bullet}}$ for the defect concentrations and mobilities used in the simulation). The situation strongly changes at high p_{O_2} , where proton uptake happens mainly by hydrogenation reaction (3) (cf. the large redox fraction of 82% as indicated in the figure), which drastically decreases the overall weight increase. There, the diffusion process is mainly ambipolar diffusion of protons and holes (= chemical diffusion of hydrogen, for which under the given conditions of high hole conductivity $D_H^{\delta} \approx D_{OH_O^\bullet}$). In such a case the H uptake constitutes a large share of the overall weight increase, and proceeds faster than the incorporation of oxygen (which, given the small weight changes and the even smaller contribution from O, is difficult to be distinguished at all from baseline drift). Thus the weight relaxation can still be fitted with a single effective diffusion coefficient, which now corresponds to D_H^{eff} and comes close to $D_{OH_O^\bullet}$, as shown in Fig. 10(c).

The alternative hypothesis that the lower weight changes upon p_{H_2O} increase in high p_{O_2} are completely caused by decreased proton uptake (but still occurring by the hydration reaction) can be discarded as it could not explain the increased effective diffusivities at high p_{O_2} . The combination of decreasing Δm and increasing D_m^{eff} with increasing p_{O_2} gives strong evidence for the gradual transition from hydration to hydrogenation.

So we can summarize that overall the numerical simulations reproduce the experimentally observed trends of overall weight changes and effective diffusion coefficients with p_{O_2}, and thus support the given interpretation of the stoichiometry relaxation kinetics although the nonideal defect chemical behavior of BSFZ (not surprising given the high defect concentrations and comparably low measurement temperatures) requires some adjustments in the input parameters.

Conclusions

The present thermogravimetric investigation shows that BSFZ incorporates a nonnegligible amount of protons (although less than barium zirconate cerate electrolyte materials). The mode of proton incorporation changes from hydration (at low p_{O_2}) to hydrogenation (at high p_{O_2}), indicating that the presence of oxygen vacancies is not necessarily required for proton uptake. The modification of the overall proton incorporation reaction is accompanied by pronounced changes in the diffusion kinetics. This findings clearly show that in such systems with more than two carriers the *complete* defect chemistry and transport behavior *must* be analyzed (the weight change after pH$_2$O increase is not necessarily uptake of water; the corresponding diffusion coefficient may differ from $D^{\delta}_{H_2O}$). Interestingly, the proton diffusivity in BSFZ is found to be in the same range as in Y-doped $BaZrO_3$ electrolyte materials. The reasons for the lower proton uptake of mixed conducting cathode materials for H^+-SOFC compared to proton conducting perovskite electrolytes (and for the variation of proton content among the potential H^+-SOFC cathode materials) deserve further investigation.

Acknowledgements: We acknowledge assistance by G. Götz and H. Hoier (XRD) and B. Baum (grinding/polishing of BSFZ pellets), all at MPI FKF Stuttgart.

References

[1] T. Norby, *Solid State Ionics* 1999, **125**, 1.
[2] K. D. Kreuer, *Solid State Ionics* 2001, **145**, 295.
[3] J. Fleig, *Ann. Rev. Mat. Res*. 2003, **33**, 361.
[4] A. Grimaud, F. Mauvy, J. M. Bassat, S. Fourcade, M. Marrony, J. C. Grenier, *J. Mater. Chem*. 2012, **22**, 16017.
[5] A. Grimaud, F. Mauvy, J. M. Bassat, S. Fourcade, L. Rocheron, M. Marrony, J. C. Grenier, *J. Electrochem. Soc*. 2012, **159**, B683.
[6] F. He, T. Wu, R. Peng, C. Xia, *J. Power Sources* 2009, **194**, 263.
[7] R. Peng, T. Wu, W. Liu, X. Liu, G. Meng, *J. Mater. Chem*. 2010, **20**, 6218.
[8] E. Fabbri, L. Bi, D. Pergolesi, E. Traversa, *Adv. Mater*. 2012, **24**, 195.
[9] L. Zhao, B. B. He, Y. H. Ling, Z. Q. Xun, R. R. Peng, G. Y. Meng, X. Q. Liu, *Int. J. Hydr. Energ.* 2010, **35**, 3769.
[10] S. Ricote, N. Bonanos, F. Lenrick, R. Wallenberg, *J. Power Sources* 2012, **218**, 313.
[11] R. O'Hayre, oral presentation at SSPC17, June 15-19 2014, Seoul, Korea
[12] K. D. Kreuer, *Ann. Rev. Mater. Res*. 2003, **33**, 333.
[13] D. Han, Y. Okumura, Y. Nose, T. Uda, *Solid State Ionics* 2010, **181**, 1601.
[14] D. Hashimoto, D. Han, T. Uda, *Solid State Ionics* 2014, **262**, 687.
[15] D. Poetzsch, R. Merkle, J. Maier, *Phys. Chem. Chem. Phys*. 2014, **16**, 16446.
[16] D. Poetzsch, R. Merkle, J. Maier, to be submitted (2015)
[17] D. Poetzsch, R. Merkle, J. Maier, *Adv. Funct. Mater*. 2015, doi:10.1002/adfm.201402212
[18] The exact boundary between predominant hydration and hydrogenation reaction in fig. 1 is given by the condition $2[V_O^{\bullet\bullet}]=[h^{\bullet}]$, which can be derived as follows: Solving eq. (2) for $[V_O^{\bullet\bullet}]$ and eq. (3) for $[h^{\bullet}]$ and taking the derivative with respect to p_{H_2O}, one obtains $\frac{\partial \ln[V_O^{\bullet\bullet}]}{\partial \ln pH_2O}=2\frac{\partial \ln[OH_O^{\bullet}]}{\partial \ln pH_2O}-1$ and $\frac{\partial \ln[h^{\bullet}]}{\partial \ln pH_2O}=\frac{\partial \ln[OH_O^{\bullet}]}{\partial \ln pH_2O}-\frac{1}{2}=\frac{1}{2}\frac{\partial \ln[V_O^{\bullet\bullet}]}{\partial \ln pH_2O}$, and correspondingly $\frac{\partial[h^{\bullet}]}{[h^{\bullet}]}=\frac{1}{2}\frac{\partial[V_O^{\bullet\bullet}]}{[V_O^{\bullet\bullet}]}$. This yields the condition $2[V_O^{\bullet\bullet}]=[h^{\bullet}]$ for the boundary where $\partial[h^{\bullet}]=\partial[V_O^{\bullet\bullet}]$.
[19] J. Maier, *J. Am. Ceram. Soc*. 1993, **76**, 1212 and 1223.
[20] J. H. Yu, J.-S. Lee, J. Maier, *Angew. Chemie Int. Ed*. 2007, **46**, 8992.
[21] H.-I. Yoo, J.-Y. Yoon, J.-S. Ha, C.-E. Lee, *Phys. Chem. Chem. Phys*. 2008, **10**, 974.
[22] H.-I. Yoo, J. I. Yeon, J.-K. Kim, *Solid State Ionics* 2009, **180**, 1443.
[23] J. H. Yu, J.-S. Lee, J. Maier, *Solid State Ionics* 2010, **181**, 154.
[24] E. Kim, H.-I. Yoo, *Solid State Ionics* 2013, **252**, 132.
[25] G.-R. Kim, H.-H. Seo, J.-M. Jo, E.-C. Shin, J. H. Yu, J. S. Lee, *Solid State Ionics* 2015 accepted
[26] While the proton flux is designated by $J_{V_O^{\bullet\bullet}}+J_{OH_O^{\bullet}}+J_{h^{\bullet}}=0$, it is important to keep in mind that in proton- and mixed conducting perovskites only the proton migrates, not the whole hydroxide ion.
[27] D. Poetzsch, PhD Thesis, University of Stuttgart, Germany, 2014.
[28] H. J. M. Bouwmeester, H. Kruidhof, A. J. Burggraaf, *Solid State Ionics* 1994, **72**, 185.
[29] B. Wei, Z. Lu, X. Q. Huang, M. L. Liu, N. Li, W. H. Su, *J. Power Sources* 2008, **176**, 1.
[30] J. Mizusaki, T. Sasamoto, W. R. Cannon, H. K. Bowen, *J. Am. Ceram. Soc*. 1983, **66**, 247.
[31] J. Mizusaki, M. Yoshihiro, S. Yamauchi, K. Fueki, *J. Sol. St. Chem*. 1985, **58**, 257.
[32] L. Wang, R. Merkle, J. Maier, *ECS Transactions* 2009, **25(2),** 2497.

[33] Solution for the 1-dimensional diffusion problem, J. Crank, in *The Mathematics of Diffusion*, Oxford University Press, New York, 1975.
[34] J. Martynczuk, K. Efimov, L. Robben, A. Feldhoff, *J. Membr. Sci.* 2009, **344**, 62.
[35] K. D. Kreuer, E. Schönherr, J. Maier, *Solid State Ionics* 1994, **70**, 278.